Cardiac Movement Estimation from Coronary Angiogram Sequences Based on Non-Rigid Motion Decomposition

S. Zheng and Y. Daoyin

Abstract—**A method for estimating cardiac dynamic performance through temporal sequences of X-ray coronary angiograms is proposed. The given data are 3D vessel skeletons, reconstructed from angiogram sequences on two approximately orthogonal views, and correspondences of these skeleton points over consecutive instants. 3D cardiac surface in terms of an extended superquadrics (ESQ) is constructed from vascular skeletons to estimate cardiac deformation. According to actual characteristic of cardiac dynamics that have been confirmed by medical observations and non-rigid motion theory, complex cardiac performances are decomposed into global and local components. Parameters of all components are estimated through motion decomposition as well as compensation. Experimental results on clinical data are illustrated and discussed in terms of expected benefits and potential limitations.**

Index Terms—**Coronary angiography, extended superquadrics, motion estimation, non-rigid motion.**

I. INTRODUCTION

CARDIAC motion analysis is fundamental to diagnose certain coronary artery diseases, related to circulation deficits or myocardial anomalies. This complex task is commonly performed by highly qualified specialists through comparing the end-systolic contour with end-diastolic contour of the ventricle and measuring the ventricular volume from ventriculograms. Since coronary arteries are spatially distributed over the myocardial surface and follow cardiac dynamics, their displacements are the same as those of the associated epicardium. The cardiac dynamic information extracted from coronary vessels has attracted increasing attention in cardiac research in recent years.

X-ray coronary angiogram is the main clinical modality to record the morphology and performances of arteries during cardiac cycles. According to 3D structure of the vascular tree reconstructed from a pair of simultaneous images acquired on left and right views, details of vessels can be observed from different views assisting doctors to make accurate diagnosis. Since in clinic LCA (left coronary artery) and RCA (right coronary artery) are always imaged separately and the morphology of LCA, covering the left ventricle (LV) is complex than RCA, LV

surface model can be recovered from 3D LCA data. Deformation of LV can be estimated and the geometrical and topological relationships among arteries and epicardium can be acquired based on the model.

Since late 1980's, coronary arterial and cardiac morphology and dynamics analysis in 3D from angiographic data have been carried out by cardiac researchers. Several cardiac shape models based on simple surface primitives have been presented, such as sphere and cylinder [1]. But they are too simple to describe complex cardiac performances. Coppini [2] recovered the cardiac surface based on spherical harmonic functions. A 3D kinetic description of heart was obtained by comparing cardiac configurations at end-diastole and end-systole. But estimation of deformation parameters, such as expansion, contraction, and twisting, is rather difficult due to the nature of representations with spherical harmonic functions. Chen and Huang [3]-[5] presented a hierarchical-decomposition based approach to model, analyze, and visualize cardiac motion using angiographic data. They suggested that both global and local motion and deformation of beating heart should be considered simultaneously to depict cardiac performance comprehensively. 3D coordinates of coronary arterial bifurcation points, reconstructed from biplane angiogram sequences, were input data. However, since the number of bifurcation points extracted from clinical angiographic images is rather limited and they are sparsely distributed over the cardiac surface, motion estimation results from such limited data are not absolutely accurate.

In this paper, a scheme for reconstructing 3D structure and dynamics of LV from sequences of 3D LCA axes is proposed. 3D vessel skeleton points are fitted onto a deformable model based on extended superquadrics (ESQ) surface to estimate cardiac deformation. Local performances are quantitatively estimated through non-rigid motion decomposition.

II. METHODOLOGY

Philips Integris CV single-plane X-ray cardiovascular cineangiography system was used to acquire data on two common used view angles in clinic, Lao46°Cran21° and Rao30°Caud24°, with a video rate of 15 frames per second throughout the cardiac cycle. The patients were asked to hold their breath immediately before each contrast injection. Parameters of the imaging device system like view angles and perpendicular distance between the X-ray
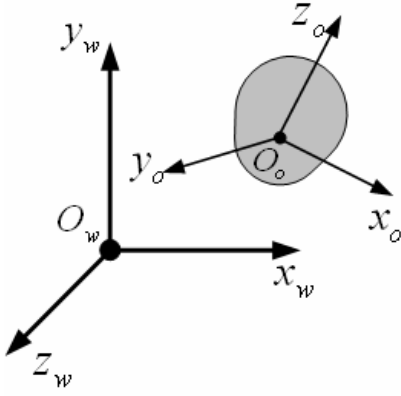
Fig. 1. Local reference system for estimating global motion.

focal spot and image planes, were recorded to characterize the imaging system. Roughly synchronous image pairs were selected with the aid of superimposed ECG signals. Original images were preprocessed to enhance the contrast. The snake based method was adopted to track main vessel branch skeletons in successive frames. The real position of the 3D vascular axis is located through snake deforming from its initial plan by minimizing an energy function that is a combination of the characteristics of two projections [6].

A. Local Reference System

Firstly, a local reference system (LRS) is built with its origin defined as the centroid of LCA skeleton data and orientation as the principal axis. As shown in Fig. 1, $O_w x_w y_w z_w$ is the fixed coordinate system for imaging system with X-ray source as the origin O_w and z_w - axis perpendicular to the imaging plane; $O_o x_o y_o z_o$ is the LRS. Suppose there are N vessel skeleton points, (x_i, y_i, z_i), $i = 1, 2, ..., N$; then the geometrical center of these points is approximated as the centroid. The principal axis is defined as an axis that goes through the centroid and the sum of the squared distance between the axis and the individual points is minimal [3].

The global translation vector T over successive instants is the difference between centroids, and the global rotation matrix R is the transformation matrix for LRS from one instant to another.

B. Modeling LV Surface

Human heart as a whole is believed to be an elastic body and its shape changes periodically over every cardiac cycle. Shape models are built at different instants from 3D coronary vessel skeletons to estimate deformations.
The use of a 3D deformable surface model can result in a faster, more robust segmentation technique which ensures a globally smooth and coherent surface [7]. Many researchers have since explored the use of deformable surface models for segmenting structures in medical image volumes. In recent years, superquadrics (SQ) have received significant attention due to compact representation and robust method for recovering 3D objects. However, the intrinsic symmetry leads to fail in modeling numerous real-world objects. Terzopoulos and Metaxas [8] formulated deformable SQ incorporating global deformations representing prominent shape features, and local deformations capturing surface details. As a result,

deformable SQ is capable of modeling non-symmetrical objects. Chen [3] used a SQ surface with tapering and twisting deformation to model LV. However, since deformable SQs are physics-based models with internal deformation energies and do not have closed form equations, they may have problems in generating an object knowledge database for object recognition. SQ surface with such simple deformations is still too simple to represent the complex shape of the heart. Zhou [9] proposed a new approach called extend superquadrics to extend SQ with exponent functions. An ESQ surface is defined as:

$$S(\theta, \phi) = \begin{bmatrix} x \\ y \\ z \end{bmatrix} = \begin{bmatrix} a_x \, sign(\cos\theta\cos\phi) |\cos\theta|^{f_1(\theta)} |\cos\phi|^{f_2(\theta)} \\ a_y \, sign(\cos\theta\sin\phi) |\cos\theta|^{f_1(\theta)} |\sin\phi|^{f_2(\theta)} \\ a_z \, sign(\sin\theta) |\sin\theta|^{f_1(\theta)} \end{bmatrix} \quad (1)$$

The implicit equation of ESQ is:

$$\left((x/a_x)^{2/f_2(\phi)} + (y/a_y)^{2/f_2(\phi)} \right)^{f_2(\phi)/f_1(\phi)} + (z/a_z)^{2/f_1(\phi)} = 1 \quad (2)$$

where, θ and ϕ are longitude and latitude angles, with $-\pi/2 \le \theta \le \pi/2$, $-\pi \le \phi \le \pi$; a_x, a_y, a_z determine the size of the surface in x, y, z directions (in object-centered coordinate system); sign(x) is a sign function; exponents $f_1(\theta), f_2(\phi)$ are functions of θ and ϕ, which are squareness parameters along z- axis and in x-y plane, respectively. ESQ can deform in any direction to model non-symmetric objects because they extend the exponents of SQ to functions of θ and ϕ. The size of coefficient set can be chosen and generally speaking, the number of coefficients is comparably smaller than that of other forms of surface primitives for describing complex shapes.

Based on features of ESQ and the complex characteristic of LV shape and deformation, an ESQ is adopted to model LV with exponent functions represented by a Bezier curve of degree three [9],

$$C(t) = \sum_{i=0}^{3} P_i B_i^3(t) = (1-t)^3 P_0 + 3(1-t)^2 t P_1 + 3(1-t)t^2 P_2 + t^3 P_3 \quad (3)$$

where $0 \le t \le 1$, $B_i^3(t)$ is the Bernstein polynomials of degree three, and Pi are control points.

After transformed to the LRS, vessel skeleton points are fitted to an ESQ surface through minimizing an error-of-fit function[9]

$$EOF = \sum_{i=1}^{N} [F(x_i, y_i, z_i) - 1]^2 \quad (4)$$

where $F(x, y, z)$ is the inside-outside function,

$$F(x, y, z) =$$
$$\left((x/a_x)^{2/f_2(\phi)} + (y/a_y)^{2/f_2(\phi)} \right)^{f_2(\phi)/f_1(\theta)} + (z/a_z)^{2/f_1(\theta)} \quad (5)$$

where $\theta = arctg\left(z / \sqrt{x^2 + y^2} \right)$ and $\phi = arctg(y/x)$. This function determines the position of a given point (x, y, z) relative to the surface: if $F(x, y, z) > 1$, the point is outside the surface; if $F(x, y, z) = 1$, it is on the surface; if $F(x, y, z) < 1$, it is inside the surface. The problem of fitting ESQ has to be formulated as a non-linear least-square problem. Levenberg-Marquardt non-linear optimization method is then utilized to accomplish the minimization.
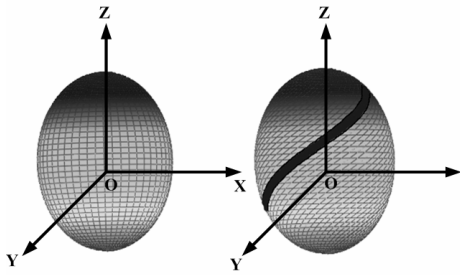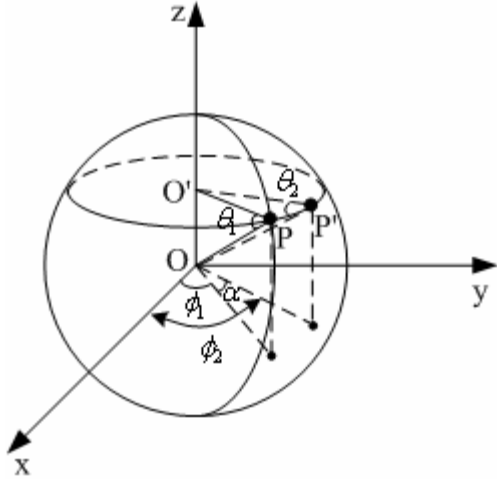
Fig. 2. Twisting deformation around z- axis.

Fig. 3. Relationship of spherical coordinates for points before and after twisting.

C. Estimating Global Deformation

Among various deformations, such as expansion, contraction, twisting, bending and local stretching, the deformation due to expansion or contraction accounts for a commanding high percentage. Parameters, depicting expansion or contraction in three orthogonal directions, can be estimated through comparing size coefficients of ESQ models at consecutive instants. The transformation equation for expansion/contraction deformation is:

$$X = \lambda_x x, Y = \lambda_y y, Z = \lambda_z z \tag{6}$$

where (x, y, z) and (X, Y, Z) are coordinates of a point before and after deformation defined in the LRS; $\lambda_x, \lambda_y, \lambda_z$ are expansion/contraction scale factors in three orthogonal directions. Suppose that size parameters of ESQs at two instants are $(a_x{}^1, a_y{}^1, a_z{}^1)$ and $(a_x{}^2, a_y{}^2, a_z{}^2)$; then the scale factors are:

$$\lambda_x = a_x{}^2 / a_x{}^1, \ \lambda_y = a_y{}^2 / a_y{}^1, \ \lambda_z = a_z{}^2 / a_z{}^1 \tag{7}$$

Twisting deformation can be expressed as a non-uniform rotation with one coordinate component invariant and others rotating about that one (Fig. 2). For example, twisting around z- axis can be considered as [10]:

$$\begin{cases} \alpha = K_\omega z, \quad c_\alpha = \cos\alpha \quad s_\alpha = \sin\alpha \\ X = x c_\alpha - y s_\alpha, \quad Y = x s_\alpha + y c_\alpha, \quad Z = z \end{cases} \tag{8}$$

where α is the rotation angle around z- axis and K_ω is the twisting parameter. Since global twisting deformation over consecutive instants is approximately uniform, the twisting parameter should approximately be a constant.

Suppose that the Cartesian coordinate of a point P on the surface at instant t is $(x_1(\theta_1, \phi_1), y_1(\theta_1, \phi_1), z_1(\theta_1, \phi_1))$, and

at $t+1$ it moves to $P'(x_2(\theta_2, \phi_2), y_2(\theta_2, \phi_2), z_2(\theta_2, \phi_2))$. Expansion or contraction deformation should be compensated before estimating twisting parameters. After such compensation, the position of P' is

$$P''(x_2(\theta_2, \phi_2)/\lambda_x, y_2(\theta_2, \phi_2)/\lambda_y, z_2(\theta_2, \phi_2)/\lambda_z)$$

As shown in Fig. 3, the relationship between $P(\theta_1, \phi_1)$ and $P''(\theta_2, \phi_2)$ in the spherical coordinate system can be deduced:

$$\theta_2 = \theta_1, \phi_2 = \phi_1 + \alpha \tag{9}$$

According to (1), (8) and (9), the twisting parameter K_ω can be calculated.

D. Estimating Local Motion

Correspondences of 3D vessel skeleton points over consecutive instants can be acquired by estimating their motion between consecutive instants[11]. After global motion and deformation are compensated according to estimated parameters, the difference between corresponding points at consecutive instants is local displacement without considering computation errors.

As known, coronary vessel points are sparely and biasedly distributed over the epicardial surface. In order to analyze local deformations, local displacements are interpolated over their neighborhood [3]. Suppose that the spherical coordinate of a given point on the model surface at instant t is $(r_t, \vartheta_t, \varphi_t)$ and its position at $t + \Delta t$, $(r_{t+\Delta t}, \vartheta_{t+\Delta t}, \varphi_{t+\Delta t})$, is to be estimated. r is the radius of a point on the ESQ surface obtained in Section II.B:

$$r(\vartheta, \varphi) = [\left(a_x (\sin\vartheta)^{f_1(\vartheta)} (\cos\varphi)^{f_2(\varphi)}\right)^2 + \left(a_y (\sin\vartheta)^{f_1(\vartheta)} (\sin\varphi)^{f_2(\varphi)}\right)^2 + \left(a_z (\cos\vartheta^{f_1(\vartheta)})\right)^2]^{\frac{1}{2}} \tag{10}$$

The local displacement field at each instant is also expressed as the spherical coordinate variation, $\Delta\vartheta, \Delta\varphi$.

$$\begin{cases} \vartheta_{t+\Delta t} = \vartheta_t + \Delta\vartheta(\theta_t, \phi_t) \\ \varphi_{t+\Delta t} = \varphi_t + \Delta\varphi(\theta_t, \phi_t) \end{cases} \tag{11}$$

The functions, $\Delta\vartheta(\vartheta, \varphi)$ and $\Delta\varphi(\vartheta, \varphi)$, are approximated by spherical harmonic functions, where the sample data are local displacements of given vessel skeleton points. This problem can be solved by applying linear least-squares method. As a result, for any given point on the ESQ surface, the coordinate of the correspondent point at the next instant can be calculated.

Helmholtz Theorem states that locally, the motion of a sufficiently small volumetric element of a deformable body can be decomposed into the sum of a translation, a rotation, and a deformation in three orthogonal directions and the motion is uniform in the volumetric element [12]. The mathematical expression for the motion field of a volumetric element belonging to the non-rigid body is:

$$[x_i' \quad y_i' \quad z_i']^T = T + R \cdot E \cdot [x_i \quad y_i \quad z_i]^T \tag{12}$$

where $P_i(x_i, y_i, z_i)$ is a point within the volumetric element at instant t and $P_i'(x_i', y_i', z_i')$ is its correspondence at $t+1$. $T = [a \quad b \quad c]^T$ is the translation vector in three orthogonal directions. R is the product of the rotation matrices around x-, y-, z-axis
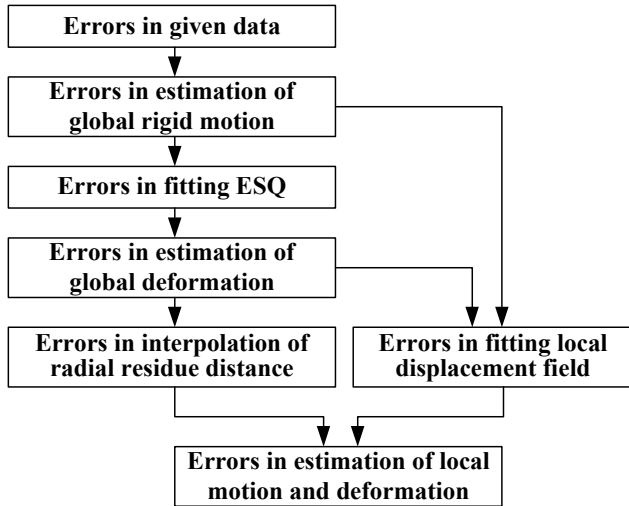
Fig. 4. Possible errors produced in the estimation algorithm and the transferring relation.

$$R = \begin{bmatrix} \cos\gamma & \sin\gamma & 0 \\ -\sin\gamma & \cos\gamma & 0 \\ 0 & 0 & 1 \end{bmatrix} \begin{bmatrix} \cos\beta & 0 & -\sin\beta \\ 0 & 1 & 0 \\ \sin\beta & 0 & \cos\beta \end{bmatrix} \begin{bmatrix} 1 & 0 & 0 \\ 0 & \cos\alpha & \sin\alpha \\ 0 & -\sin\alpha & \cos\alpha \end{bmatrix} \quad (13)$$

where α, β, γ are rotation angles around x-, y-, z- axis, respectively. For simplification, small angle rotation can be assumed to obtain the approximate representation of R :

$$R \approx \begin{bmatrix} 1 & \gamma & -\beta \\ -\gamma & 1 & \alpha \\ \beta & -\alpha & 1 \end{bmatrix} \quad (14)$$

$E = [e_{ij}], (i = 1,2,3; j = 1,2,3)$ is a deformation matrix which is symmetric with $e_{12} = e_{21}$, $e_{13} = e_{31}$, $e_{32} = e_{23}$. So among all nine components of E, there are six independent ones, $e_{11}, e_{12}, e_{13}, e_{22}, e_{23}, e_{33}$. In summary, there are totally twelve unknowns in (12), $(a, b, c, \alpha, \beta, \gamma, e_{11}, e_{12}, e_{13}, e_{22}, e_{23}, e_{33})$. For each pair of correspondences, three equations can be established:

$$\begin{cases} x_{i+1} = a + (1+e_{11})x_i + (-\gamma + e_{12})y_i + (\beta + e_{13})z_i \\ y_{i+1} = b + (\gamma + e_{21})x_i + (1+e_{22})y_i + (-\alpha + e_{23})z_i \\ z_{i+1} = c + (-\beta + e_{31})x_i + (\alpha + e_{32})y_i + (1+e_{33})z_i \end{cases} \quad (15)$$

Hence, in order to determine all twelve unknowns, at least four point correspondences within the local volumetric element are required.

III. EXPERIMENT RESULTS AND DISCUSSION

A. Error Analysis

Errors are analyzed and calculated in this section to evaluate the method. Through analyzing the overall calculating process, possible errors existing in every step and the transferring relation are shown in Fig. 4.

Suppose that coordinates of skeleton points at the first instant are $X_1 = [x_i^1 \quad y_i^1 \quad z_i^1]^T$ and those at the second instant are $X_2 = [x_i^2 \quad y_i^2 \quad z_i^2]^T$. Upon compensation of global rigid motion for X_2 and then transformation of it to the LRS at the first instant, global deformation is compensated to obtain $mX_2 = [mx_i^2 \quad my_i^2 \quad mz_i^2]^T$. Transforming X_1 to its LRS to obtain $mX_1 = [mx_i^1 \quad my_i^1 \quad mz_i^1]^T$, differences between correspondences in x, y, z directions are:

(a)

(b)

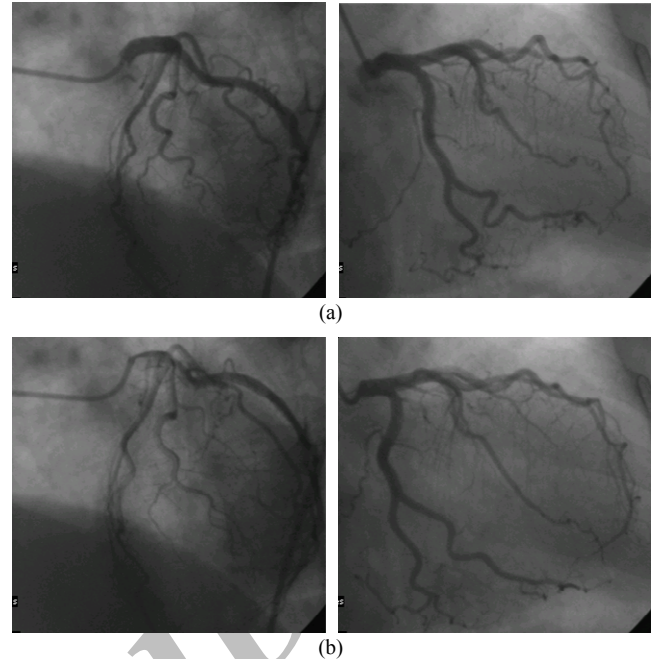Lao46° Cran21°   Rao30° Caud24°

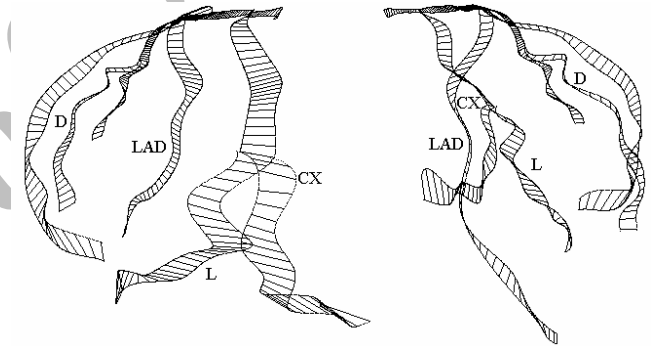Fig. 5. Original image pairs of LCA at two consecutive instants, (a) Instant 1, and (b) Instant 2.

Fig. 6. 3D vessel skeletons and motion vectors at consecutive instants reconstructed from Fig. 5.

TABLE I
STATISTIC RESULTS OF DISPLACEMENTS FOR 3D VESSEL SKELETON POINTS SHOWN IN FIG. 6

Statistic results of displacements	Value (mm)
Maximum displacement	14.6227
Minimum displacement	0
Average displacement	5.0829

$$\begin{cases} \Delta x_i = mx_i^2 - mx_i^1 \\ \Delta y_i = my_i^2 - my_i^1 \\ \Delta z_i = mz_i^2 - mz_i^1 \end{cases} \quad (16)$$

The distance between correspondences is

$$\Delta d_i = \sqrt{(\Delta x_i)^2 + (\Delta y_i)^2 + (\Delta z_i)^2} \quad (17)$$

where $i = 1,2,...,N$.

Differences described by (16) and (17) are totally due to local motion and deformation without considering computation errors. However, in the actual estimation process, there are inevitable errors in each step and given vessel skeleton points due to 3D reconstruction. Under such condition, differences in (16) and (17) include two parts: local displacements and computation errors. Both cannot be completely separated from each other.

Fig. 7. 3D view of the LV model estimated from vessel skeletons shown in Fig. 6.
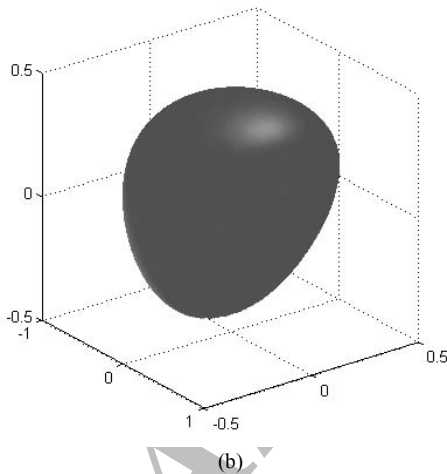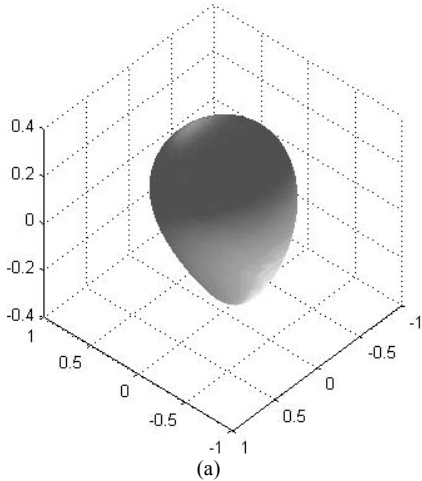

(a)

(b)

Fig. 8. 3D view of the LV shape models estimated from the 3D vessel skeletons at (a) ED, and (b) ES.

TABLE II
MEASUREMENT OF ERRORS (IN MM) IN MOTION ESTIMATION FROM VESSEL SKELETON DATA SHOWN IN FIG. 6

Statistic results of errors	Value (mm)
Maximum error	9.8252
Minimum error	0.2011
Average error	5.1391
Root mean squared error	0.0978
Standard deviation error	2.2118

B. Results of Real Data

In this section the experimental results of the proposed method applied to real data is presented. Fig. 5 shows two image pairs of LCA at consecutive instants acquired on view angles of RAO30°CAUD24° and LAO46°CRAN21°, which were synchronized with ECG gating signal.
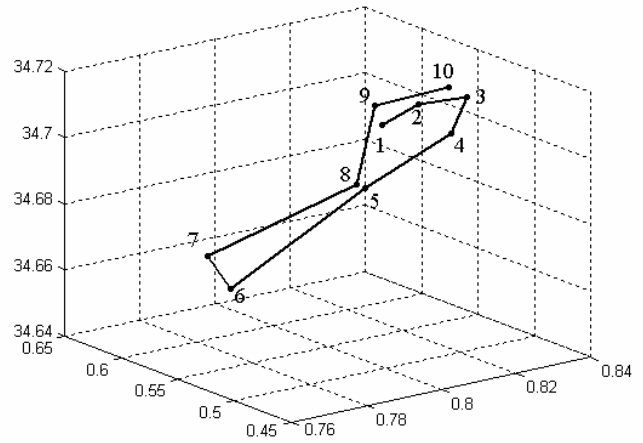

Fig. 9. 3D view of the estimated centroid trajectory (numbers on the trajectory represent instants).

Two different views of the 3D vessel skeletons reconstructed from Fig. 5 are shown in Fig. 6, where the corresponding points were connected with lines representing displacement vectors. In Table I, statistic results of displacements for total 3372 points on the 3D skeletons shown in Fig. 6 are listed.

The skeleton points at instant 1 were fitted to an ESQ surface, shown in Fig. 7. Fig. 8 shows the 3D view of the estimated LV global shape from the vessel skeletons at end-systole (ES) and end-diastole (ED).

After estimating cardiac motion and deformation parameters over the two instants, original skeleton points at the second instant are transformed according to estimated dynamic parameters. Then, estimation errors are computed by calculating differences between these transformed points and corresponding original points at the first instant, results listed in Table II.

The estimated 3D trajectory of the LV centroid along ten successive instants is shown in Fig. 9. From the trajectory it can be noticed that when one cardiac cycle ends (at the tenth instant) the centroid has a tendency to move back to its starting position (at the third instant), corresponding well to the supposed periodic motion of the heart.

IV. CONCLUSIONS

Since inadequacy of myocardial perfusion is frequently caused by coronary atherosclerosis leading to vessel lumen reduction and regional underperfusion, the estimation of the myocardial regions at risk of ischemia or infarction provides an important descriptor of the functional status of the heart and has prognostic relevance. In this paper we have presented an approach to exploit cardiac motion through estimating relevant quantitative parameters from X-ray coronary angiographic sequences. As coronary vessels are natural descriptors of cardiac surface, 3D LCA skeletons are adopted in LV surface recovering using 3D deformable surface model based on ESQ. From such a shape model, the global deformation, such as expansion, contraction, twisting, are quantitatively estimated by analyzing the variations of model coefficients over consecutive instants. The local displacement fields of points on the model surface are acquired by interpolating the local displacements of coronary vessel skeleton points.

We estimate the dynamic components of every small volumetric element belonging to the model through decomposing the local displacement field based on the well-known Helmholtz non-rigid motion theory.

In the further related work we will use color encoding technique in the description of epicardial regions at risk and corresponding deformations.

REFRENCES

[1] T. Arts and R. S. Reneman, "Dynamics of left ventricular wall and mitral valve mechanics—a model study," *Journal of Biomechanics*, vol. 22, no. 3, pp. 261-271, 1989.

[2] G. Coppini, M. Demi, P. Marraccini, and A. L'Abbate, "3D heart motion from X-ray angiography," in *IEEE Proceedings of Computers in Cardiology*, pp. 71-74, Sept. 1995.

[3] C. W. Chen, T. S. Huang, and M. Arrott, "Modeling, analysis and visualization of left ventricle shape and motion by hierarchical decomposition," *IEEE Trans. on Pattern Analysis and Machine Intelligence*, vol. 16, no.4, pp. 342-356, Apr. 1994.

[4] C. W. Chen and T. S. Huang, "Epicardial motion and deformation estimation from coronary artery bifurcation points," in *Proc. of IEEE 3rd International Conference on Computer Vision*, pp. 456-459, Dec. 1990.

[5] C. W. Chen, T. S. Huang, "Left ventricle motion analysis by hierarchical decomposition," in *Proc. of IEEE 3rd International Conference on Acoustics, Speech, and Signal Processing*, vol. 3, pp. 273-276, Mar. 1992.

[6] C. Canero, P. Radeva, R. Toledo, J. J. Villanueva, and J. Mauri, "3D curve reconstruction by biplane snakes," in *Proc of 15th International Conference on Pattern Recognition*, vol. 4, pp. 563-566, Sep. 2000.

[7] T. McInerney and D. Terzopoulos, "Deformable models in medical image analysis: a survey," *Medical Image Analysis*, vol. 1,no. 2, pp. 91-108, 1996.

[8] D. Terzopoulos and D. Metaxas, "Dynamic 3D models with local and global deformations: Deformable superquadrics," *IEEE Trans. on Pattern Analysis and Machine Intelligence*, vol. 13, no. 7, pp. 703-714, Jul. 1991.

[9] L. Zhou and C. Kambhamettu, "Extended superquadrics with exponent functions: modeling and reconstruction," in *Proc. IEEE Computer Society Conference on Computer Vision and Pattern Recognition*, vol. 2, pp. 73-78, Jun. 1999.

[10] T. W. Sederberg and S. T. Parry, "Free-form deformation of solid geometric models," in *Proc. of the 13th Annual Conference on Computer Graphics and Interactive Techniques,* vol. 20, no. 4, pp. 151-159, Aug. 1986.

[11] S. Y. Chen, J. D. Carroll, "Kinematic and deformation analysis of 4-D coronary arterial trees reconstructed from cine angiograms," *IEEE Trans. on Medical Imaging*, vol. 22, no. 6,pp. 710-721, Jun. 2003.

[12] A. Sommerfeld, *Mechanics of Deformable Bodies*, New York Academic, 1950.

S. Zheng received the B.Sc. degree in optical technology and opto-electronic instrument, and M.Sc. and Ph.D. degrees in optical engineering from Tianjin University, P. R. China, in 1999, 2002, and 2004, respectively.

She is now a post-doctor in the School of Precision Instrument and Opto-electronic Engineering at Tianjin University. Her research interests include medical image processing and pattern recognition.

Y. Daoyin was born in Anhui, P.R.China, in 1945. He received the M.Sc. degree in optical engineering from Tianjin University, P. R. China, in 1984.

He is now a Professor in the School of Precision Instrument and Opto-electronic Engineering at Tianjin University. His research interests include optical fiber and opto-electronic instrument design, medical instrument, and medical image processing.